This is a preprint, the final version is subject to change, of the American Mineralogist (MSA)
Cite as Authors (Year) Title. American Mineralogist, in press.
DOI: https://doi.org/10.2138/am-2018-6351

Revision 2, correction date: January 31, 2018

Quantitative determination of Al/Si order in sillimanite by high angular resolution electron channeling X-ray spectroscopy

Yohei IGAMI[1,*], Takahiro KURIBAYASHI[2], and Akira MIYAKE[1]

[1]Department of Geology and Mineralogy, Graduate School of Science, Kyoto University, Kyoto 606-8502, Japan

[2]Department of Earth Science, Graduate School of Science, Tohoku University, Sendai 980-8578, Japan

*Corresponding author. E-mail: y-igami@kueps.kyoto-u.ac.jp

Abstract

Sillimanite is a polymorph of Al_2SiO_5 that is widely used as an indicator of pressures and temperatures reached during metamorphism. The degree of disorder in the double chains of SiO_4 and AlO_4 tetrahedra in sillimanite, particularly at high temperatures, is of interest as a factor in the phase relations of the Al_2SiO_5 polymorphs. We determined the Al/Si order parameter (Q) of sillimanite from Rundvågshetta, Antarctica, by the High Angular Resolution Electron Channeling X-ray Spectroscopy (HARECXS) method using transmission electron microscopy with energy dispersive X-ray spectrometry. HARECXS profiles were successfully obtained from regions ~1 μm in diameter by automated control

This is a preprint, the final version is subject to change, of the American Mineralogist (MSA)
Cite as Authors (Year) Title. American Mineralogist, in press.
DOI: https://doi.org/10.2138/am-2018-6351

of beam tilting and X-ray detection. The obtained Q value was close to that previously estimated by single-crystal X-ray diffraction. Moreover, the Q values of annealed samples were obtained while avoiding interference from mullite or SiO_2-rich glass domains formed by annealing. For quantitative determination of Q, we also performed theoretical calculations of HARECXS profiles and evaluated sample thicknesses by convergent-beam electron diffraction. The experimentally obtained profiles were successfully fitted by a linear combination of simulated profiles of completely ordered and completely disordered sillimanite, which yielded Q values. The Q values obtained from 18 measurements showed no effect from differing sample thicknesses. Moreover, the results from annealed samples showed that Q decreases continuously with increasing annealing temperature. The temperature dependence of Q values, formulated by least-squares fitting on the basis of the Bragg-Williams approximation, yielded a transition temperature from order to disorder at 1727 °C. The obtained curve is more accurate at high temperatures than previous estimates. It indicates that the sample material reached peak temperatures greater than ~1000 °C, which is close to previous estimates of the peak metamorphic temperature of Rundvågshetta sillimanite. This study also implies that the HARECXS method is suitable for accurate analyses of other natural samples with complicated microtextures.

Keywords: ALCHEMI, HARECXS, transmission electron microscope, sillimanite, Al/Si-disordering

This is a preprint, the final version is subject to change, of the American Mineralogist (MSA)
Cite as Authors (Year) Title. American Mineralogist, in press.
DOI: https://doi.org/10.2138/am-2018-6351

Introduction

Sillimanite is one of Al_2SiO_5 polymorphs that are valuable as indicators of the pressure and temperature experienced by metamorphic rocks. The crystal structure of sillimanite consists of AlO_6 octahedral chains that are linked with double chains of SiO_4/AlO_4 tetrahedra oriented parallel to the *c*-axis. The tetrahedral Si/Al chains are usually ordered, but it has been suggested that they become disordered at high temperatures (e.g., Zen 1969; Holdaway 1971; Greenwood 1972). Disordering of Al and Si tetrahedra in sillimanite has been studied for its possible effects on phase relations of the Al_2SiO_5 polymorphs. Therefore, annealing experiments since the 1970s have sought to determine the Al/Si order parameter (Q) at high temperatures (e.g., Navrotzsky et al. 1973), but quantitative determinations have had poor success. The main problem is the difficulty of separating sillimanite from microscopic precipitates of mullite and SiO_2-rich glass, which appear in sillimanite at temperatures greater than 1200 °C (e.g., Tomba et al. 1999; Igami et al. 2017). Transmission electron microscope (TEM) observations of sillimanite heated to high temperatures have shown that the mineral is partly transformed to mullite ($Al_2[Al_{2+2x}Si_{2-2x}]O_{10-x}$, $x \approx 0.17–0.59$) with glass inclusions (e.g., Holland and Carpenter 1986; Raterron et al. 1999, 2000; Rahman et al. 2001). These textures are too fine for the spatial resolution of a scanning electron microscope (SEM) combined with energy dispersive X-ray spectrometry (EDS). X-ray diffraction (XRD) and neutron diffraction experiments cannot distinguish these coexisting phases from sillimanite because glasses do not show clear diffraction peaks and mullite is crystallographically very similar to sillimanite. Moreover, the similarity of Al and Si in their X-ray scattering factors makes

63 them difficult to determine Q by XRD.

64 Spence and Taftø (1983) developed the ALCHEMI (Atom Location by
65 CHanneling-Enhanced MIcroanalysis) analytical method in which TEM-EDS is used to
66 determine the crystallographic sites of impurity elements in crystals on the basis of
67 channeling-enhanced X-ray emissions. This method uses TEM to analyze micrometer-sized
68 regions and can distinguish elements with similar atomic number by EDS. However,
69 ALCHEMI is specialized for site determination of impurity elements in the crystals that
70 consist of the atomic planes on which two host elements arranged separately, in general.
71 Therefore, it is not applicable to the determination of order degree between mixed two
72 cations, including Al/Si order in sillimanite. However, improvements in ALCHEMI have
73 subsequently led to the HARECXS (High Angular Resolution Electron Channeling X-ray
74 Spectroscopy) method, which is suitable for wider application (e.g., Soeda et al. 2000;
75 Yasuda et al. 2006, 2007; reviewed by Muto and Ohtsuka 2017). HARECXS acquires
76 many EDS measurements as the direction of the incident electron beam is continuously
77 varied to yield X-ray intensity profiles of the elements against beam tilting. Because such
78 profiles can be precisely simulated, if the crystallographic structure is fully known, by
79 using the program ICSC (Oxley and Allen 2003) based on dynamic electron
80 elastic/inelastic scattering theory, HARECXS can be applied to crystals with complex
81 structure. Although HARECXS is not yet a fully quantitative procedure, we expected it to
82 provide improved quantitative determinations of Q in sillimanite.

83 In this study, we used HARECXS for quantitative determination of Q in a
84 sillimanite sample. The same sample was also examined by single-crystal XRD to evaluate

This is a preprint, the final version is subject to change, of the American Mineralogist (MSA)
Cite as Authors (Year) Title. American Mineralogist, in press.
DOI: https://doi.org/10.2138/am-2018-6351

the suitability of this HARECXS application. Annealed samples of the same sillimanite were then examined by HARECXS to investigate the effect of heating on Q in sillimanite suggested by theoretical studies (e.g., Zen 1969; Holdaway 1971; Greenwood 1972).

Experimental methods

Samples

Our starting material was sillimanite crystals approximately 2 mm across separated from cordierite-bearing rock collected in Rundvågshetta, East Antarctica (sample RVH92011102A, Kawasaki et al. 1993, 2011). The crystals were optically homogeneous and prismatic, with a chemical composition of $Al_{1.99}Fe_{0.01}Si_{1.00}O_5$ as determined with a SEM-EDS system (JEOL JSM-7001F SEM, Oxford Inca EDS). Sillimanite from the same locality, measured with a JEOL JCXA-8800 SEM at Ehime University (Kawasaki et al. 2011), had a similar composition. Because the amount of impurity is sufficiently small, we assume that the impurity does not affect in our analysis and the composition of this sample is Al_2SiO_5.

Single-crystal XRD measurement of the starting material

We investigated a single sillimanite crystal using an automated four-circle X-ray diffractometer (Rigaku, AFC-7S, Tohoku University) with monochromatized MoKα radiation (λ = 0.71069 Å, 50 kV, 20 mA). See Table 1 for a summary of the measurement

and its results. The cell parameters were determined from 22 centered reflections in the 2θ range between 21° and 29°. The structure was refined by using reflection data from $F_o > 4\sigma(F_o)$ and diffraction intensities measured over the range 2θ = 3–60° in the quadrant of reciprocal space (h = –10→10, k = 0→10, l = 0→8) by the 2θ – ω scan method. After making Lorentz polarization corrections, we averaged the intensities of symmetrically equivalent reflections in the Laue group 2/*m*2/*m*2/*m* to produce a set of 413 unique data. No crystal absorption correction was applied given the crystal's small size and low absorption coefficient. The structure was calculated using the SHELXL-97 program (Sheldrick 1997). The initial parameters of sillimanite with space group *Pbnm* were from Winter and Ghose (1979), and neutral atom scattering factors were used for all atoms. In addition to fractional atom coordinates, the site occupancies of tetrahedral sites (Al2, Si) were refined to evaluate *Q*. However, the site occupancies refined by peak intensities alone may not be accurate because X-ray scattering factors of Al and Si are so similar. Instead, it is common practice to determine the Al content in the O-tetrahedra of aluminum silicates from the linear relation between average T–O distance and Al content in tetrahedra (e.g., Smith and Bailey 1963). Therefore, in this study we estimated the Al content in tetrahedral sites also by comparison of T–O distance with previous studies. Bish and Burnham (1992) also attempted to estimate the Al content in tetrahedral sites from existing sillimanite data, obtaining results consistent with Al occupancies refined from neutron diffraction patterns.

Annealing experiment

Sillimanite crystals were placed in a platinum crucible and annealed in a muffle

129 furnace at five different combinations of temperature and time (1090 °C for 1255 h, 1140
130 °C for 1512 h, 1373 °C for 300 h, 1476 °C for 90 h, and 1530 °C for 5 h). The temperature
131 was measured with a $Pt_{70}Rh_{30}$–$Pt_{94}Rh_6$ (B-type) thermocouple placed at the top of the
132 sample space in the furnace. The run temperature, controlled by the thermocouple, was kept
133 constant within ±1 °C of the nominal value. After heating, samples were allowed to cool to
134 room temperature.
135
136 **Preparation for TEM analysis**
137 Sections for TEM examination were prepared from the starting material and
138 annealed samples using a focused ion beam apparatus (FEI Quanta 200 3DS or Helios
139 NanoLab G3 CX). Predefined areas measuring 15 μm × 2 μm were coated with Pt, the
140 surrounding areas were removed to a depth of ~10 μm using a Ga^+ ion gun, and then the
141 sections were cut off and mounted on a TEM grid. The extracted sections were thinned to a
142 thickness of 70–350 nm using a Ga^+ ion beam at 30 kV with beam currents of 0.1–3 nA.
143 The final processing used a Ga^+ ion beam at 5 kV with a beam current of 48 pA to remove
144 amorphous layers on the surface of the sections.
145
146 **TEM observations**
147 Before conducting the HARECXS observations, we observed the sillimanite
148 sections using a TEM (JEOL, JEM-2100F) operated at 200 kV, paying particular attention
149 to the presence of mullite. Images were recorded by a CCD camera (Gatan, Orius SC200D).
150 Crystallographically, mullite (space group: *Pbam* (No. 55), cell parameters: a = 7.54336Å,

151 b = 7.69176Å, c = 2.88402Å; Balzar and Ledbetter 1993) is very similar to sillimanite
152 (space group: *Pbnm* (No.62), cell parameters: a = 7.4883Å, b = 7.6808Å, c = 5.7774Å;
153 Winter and Ghose 1979), but mullite formation in sillimanite can be identified by the
154 presence of glass phases rich in SiO_2 that should be formed with mullite (e.g., Holland and
155 Carpenter 1986; Raterron et al. 1999, 2000; Rahman et al. 2001). The mullite formation is
156 also distinguished by its selected area electron diffraction (SAED) pattern, because there is
157 a periodic difference between the two phases: Al/Si configuration in the tetrahedral sites is
158 ordered (alternated along c-axis) in sillimanite whereas it is disordered in mullite. This
159 Al/Si alternation in the tetrahedral sites along c-axis can be identified by the reflections
160 with l = odd (2n+1) of sillimanite. These reflections are invisible in mullite because of
161 reduction of the Al/Si alternation, although these reflections are no longer "l = odd"
162 reflections in mullite because the c-axial length of mullite is also no longer half the size as
163 that of sillimanite. For simplification, we indexed all the SAED patterns based on the
164 standard cell of sillimanite. In this case, the "l = odd reflections" are typical in sillimanite
165 but are absent in mullite. Therefore, we also observed the sections by dark field imaging
166 taken from the l = odd reflections of sillimanite.
167
168 **HARECXS measurements**
169 HARECXS profiles (X-ray intensities of Al-K, Si-K and O-K vs. beam tilting
170 angle) were obtained for each sillimanite section by using a TEM-EDS system (JEOL
171 JEM-2100F, JED-2300T) operated in the beam-rocking mode with a 200 keV electron
172 beam (Fig. 1), following Muto and Ohtsuka (2017). The change in EDS spectra in response

to beam tilting was observed by using electron channeling along the (202) plane, on which Al and Si tetrahedra are arranged separately in ordered sillimanite but are mixed in disordered sillimanite (Fig. 2a). In such condition, the HARECXS profiles are expected to change the most significantly with Al/Si disordering. Firstly, the samples were tilted to the condition where only the 101 systematic row reflections were excited and other reflections were possibly not excited (Fig. 2b). Then, the measurement was performed by automated control of beam tilting and X-ray detection. The beam tilting was controlled with a small step in the direction of the 101 systematic row reflections including from $\bar{8}0\bar{8}$ to 808 Bragg conditions. The convergent angle of the incident beam was set to 0° (parallel beam) by checking diffraction spots to emphasize the channeling phenomenon. In this condition, our TEM illuminated a region ~1 μm in diameter, allowing us to analyze sillimanite regions without mullite or glass.

Convergent-beam electron diffraction (CBED) patterns were also obtained from the measurement region to estimate the thickness of the sample, which is known to affect HARECXS profiles. The sample thickness was determined by comparing obtained and simulated CBED patterns, calculated with the program MBFIT (Tsuda and Tanaka 1999).

Simulation of HARECXS profiles

We evaluated the observations by producing simulated HARECXS profiles with the program ICSC (Oxley and Allen 2003). We used structural parameters of sillimanite from Winter and Ghose (1979), and the degree of Al/Si order was varied by manipulating the site occupancies of tetrahedral sites. In the calculation of inelastic scattering process, the sample

thickness determined from CBED patterns was used as an input parameter.

This is a preprint, the final version is subject to change, of the American Mineralogist (MSA)
Cite as Authors (Year) Title. American Mineralogist, in press.
DOI: https://doi.org/10.2138/am-2018-6351

Results and discussion

Single-crystal XRD of the starting material

The results of the structural refinement of the starting material from XRD data, which converged to a final $R1$ factor of 3.19%, are listed in Tables 1 and 2. The refined site occupancy was 96.8% Al with 3.2% vacancy in the Al2 site, and 96.5% Si with 3.5% vacancy in the Si site. This is not consistent with chemical composition obtained by SEM-EDS. This indicates that the site occupancies cannot be determined accurately from peak intensities alone, as expected. Instead, we estimated the site occupancies by comparison of T–O distance with various other sillimanite, following previous studies (Bish and Burnham, 1992). Table 3 shows that the average distances of the Al2–O and Si–O bonds in tetrahedra, calculated from atomic positions, are close to those reported by Peterson and McMullan (1986). Among previous studies, Burnham (1963) reported the most ordered trend of average T–O distances; therefore, we used those results for our estimates under the assumption that the sillimanite of Burnham (1963) was a perfectly Al/Si-ordered sillimanite (i.e., $Q = 1$). Figure 3 shows the linear relationship from Burnham (1963) between Al content in tetrahedral sites and bond distance of sillimanite, with Al content in the Si site plotted as zero and Al content in the Al2 site plotted as one. The line through these two points is expressed by the relation $y = 6.4516x - 10.418$. This relation compares favorably with the work of Jones (1968), who showed that data from feldspar and other framework silicates fit the relations $y = 6.3481x - 10.178$ and $y = 6.4116x - 10.282$, respectively. Applying the relation in Figure 3 to our sillimanite data yields a proportion of 5.8(19)% Al in the Si site and 94.3(19)% Al in the Al site, for a Q value of 0.88(4). This

result also agrees with the bulk composition of tetrahedral sites, in which Si:Al = 1:1.

TEM observations and SAED patterns of untreated and annealed samples

TEM images of the starting material showed no characteristic textures such as antiphase boundaries, lamellae, or inclusions, and the SAED pattern displayed diffraction intensities from sillimanite alone (Fig. 4). However, in a sample heated at 1530 °C for 5 h, a dark-field TEM image taken from 111 reflection of sillimanite showed dark-contrast regions containing small inclusions elongated in the direction of the *c*-axis of the host sillimanite (Fig. 5). This texture resembles that resulting from mullite formation, as reported by previous TEM studies (e.g., Raterron et al. 1999, 2000; Rahman et al. 2001), and indicates that the dark region consists of mullite + SiO_2-rich glass. These mullite regions were also observed in a sample heated at 1476 °C for 90 h and in a sample heated at 1373 °C for 300 h, but they were not observed in samples heated at 1140 °C for 1512 h and at 1090 °C for 1255 h. This result is consistent with the 1200 °C formation temperature of mullite in sillimanite, as previously determined from high-resolution XRD analysis of annealed sillimanite (Igami et al. 2017). However, all samples retained regions of sillimanite that displayed l = odd reflections in their SAED patterns, which indicates that their Al/Si distribution was not completely disordered.

HARECXS profiles of the starting material

HARECXS profiles of the starting material were obtained at 18 points in two sections of differing thicknesses. Although these profiles displayed significant differences

(Fig. 6), the difference is thought to reflect the differences in sample thickness rather than differences in Q, as suggested by the differences in CBED patterns (Fig. 6). This result clearly shows the importance of accounting for sample thickness in quantitative determinations of the order parameter by HARECXS. In this study, thicknesses determined by the CBED method corresponded to the calculated HARECXS profiles.

For traditional ALCHEMI, 1/4–3/4 of the extinction distance (ξ) is acknowledged as suitable sample thickness (Buseck and Self, 1992). The extinction distance of the 101 reflection of sillimanite can be calculated using the structural parameters from Winter and Ghose (1979), to be ξ_{101} = 887nm. Therefore, the suitable sample thickness of this study is roughly expected as 222–665nm. Our HARECXS results agree with this value; for example, gradients of the profiles at the thickness of ~380nm (Fig. 7, right) is larger than those of the thickness of ~80nm (Fig. 7, left). This means that the measurement at the region of the thickness of ~380nm is expected to provide more precise result because of larger channeling effect than that of the thickness of ~80nm.

The order parameter Q was determined by fitting with linear combinations of two simulated profiles, f_i calculated assuming complete order (Q = 1) and g_i calculated assuming complete disorder (Q = 0), where i = O, Al, or Si. The linear-combination profiles F_i are expressed as

$$F_i = a_i(Qf_i + (1 - Q)g_i) + b_i,$$

where a_i is a scale factor and b_i is the background value. The Q parameter in this expression, corresponding to the contribution ratio of f_i and g_i, was determined by least-squares fitting of observed profiles of O, Al, and Si to their respective F_i. The scale and offset of the

This is a preprint, the final version is subject to change, of the American Mineralogist (MSA)
Cite as Authors (Year) Title. American Mineralogist, in press.
DOI: https://doi.org/10.2138/am-2018-6351

263 horizontal axis of the HARECXS profiles were also optimized at the time of this fitting.

264 The HARECXS profile with optimized Q shown in Figure 6 along with linear
265 combination profiles with Q = 1, 0.9, 0.8, …, 0, indicates that profiles were successfully
266 reproduced by the linear combination model. The Q values determined from each of our 18
267 measurement points (Table 4 and Fig. 7a) were consistent, averaging 0.80(1), despite the
268 widely varying thickness of the starting material.

269

270 **Comparison of results between HARECXS and XRD**

271 The average Q value of 0.80(1) for sillimanite determined by HARECXS is roughly
272 consistent with the result of 0.88(4) determined by XRD, but there is a slight discrepancy.
273 Oxley and Allen (2003) noted that a term for absorptive scattering of the incident electron
274 beam other than thermal diffuse scattering (additional mean absorption λ_{ABS}) must be added
275 to calculations to make experimental and observed HARECXS profiles agree. They
276 reported that λ_{ABS} = 1300 Å (mean free path equivalent) was required to ensure agreement
277 between the calculated and experimental HARECXS profile of Matsumura et al. (2001),
278 obtained from a specimen of spinel ($MgAl_2O_4$) 1800 Å thick by using a 120 keV incident
279 electron beam. They mentioned that λ_{ABS} may also simulate the effect of experimental
280 factors, such as uncertainty in sample thickness, specimen drift, or beam convergence.
281 Therefore, we tested three different values of the parameter λ_{ABS} in this study (Table 4 and
282 Fig. 7) and found that λ_{ABS} = 2500 Å yielded the best match with the XRD result of Q =
283 0.88(4). The additional term λ_{ABS} = 2500 Å for correction of systematic errors may be
284 suitable for quantitative analyses of HARECXS profiles obtained by our method.

285

286

287 **HARECXS measurements of annealed sillimanite**

288 HARECXS profiles were also obtained from annealed samples, avoiding
289 precipitation of mullite or glass inclusions, and Q values were determined by fitting
290 simulated profiles using λ_{ABS} = 2500 Å. The linear combination model successfully
291 reproduced the HARECXS profiles (Table 5 and Fig. 8). We found that annealing
292 temperatures as high as 1530 °C did not completely disorder sillimanite in the HARECXS
293 profiles (Fig. 9). This result is consistent with our SAED patterns, which displayed l = odd
294 reflections in all samples. The HARECXS results improved upon SAED patterns by
295 showing more quantitatively that Q decreased continuously from ~0.9 to ~0.5 with
296 increasing temperature.

297

298

299 **Temperature dependence of *Q* in sillimanite**

300 We used our experimental results to determine the order parameter Q as a function
301 of temperature by least-squares fitting with the Bragg-Williams model (solid line in Fig. 9).
302 This well-known model can predict how the equilibrium order parameter Q varies with
303 temperature, on the assumption that the enthalpy of cation mixing arise only from the
304 interactions between the nearest neighbor cations. We used the lowest Q value at each
305 heating temperature for the fitting, considering it to be the result closest to the equilibrium
306 disordered state. This fitting yielded a transition temperature of 1727 °C, although the real

transition temperature might be slightly lower if the samples did not reach an equilibrium disordered state. This result implies that sillimanite becomes completely disordered above approximately 1700 °C. However, at low pressures, the transformation to mullite with partial melting begins immediately at these temperatures (e.g., Tomba et al. 1999; Igami et al. 2017). Greenwood (1972) also studied Al/Si order in sillimanite and predicted values of Q as a function of temperature with the Bragg-Williams model, but that prediction was loosely constrained (between the dotted lines in Fig. 9) because experimental evidence at high temperatures was lacking. The curve established by this study is well constrained at high temperatures.

Implications

In this study, we successfully quantified the Al/Si order parameter Q in annealed sillimanite, and the results shows that Q decreases with increasing temperature. According to the Bragg-Williams Q–T curve (Fig. 9), our Q value of 0.88 ± 0.01 for the sillimanite sample from Rundvågshetta corresponds to an experienced temperature of 1000 ± 30 °C. This result is comparable to independent estimates that put the peak metamorphic temperature at Rundvågshetta higher than at least 900–1000 °C (e.g., Kawasaki et al. 1993, 2011; Harley 1998; Fraser et al. 2000). The real peak temperature may have been higher, because Q may have increased during slow cooling from the peak metamorphic stage. More exact temperature will be estimated by further experiments taking cooling rate into account. Subsequent precise experiments about temperature dependence of Q in sillimanite would

329 also shed more light on the effect of Al/Si disordering to the phase equilibria of the Al_2SiO_5
330 polymorphs, which in turn should increase the accuracy of the Al_2SiO_5 phase diagram.

331 The HARECXS method enabled us to obtain crystallographic information from a
332 ~1 μm diameter region, avoiding even the smallest interfering phases. Our results suggest
333 that HARECXS will be useful for determining site occupancies of other common
334 rock-forming minerals, such as Mg/Fe in olivine or pyroxene, and possibly for obtaining
335 new information about the formation process of minerals with complicated microtextures.
336

337 **Acknowledgments**

338 We are grateful to Shunsuke Muto, Masahiro Ohtsuka (Nagoya University), Kenji Tsuda
339 (Tohoku University), and Shoichi Toh (Fukuoka University) for their help and advice on
340 TEM analyses. We also thank Toshisuke Kawasaki (Ehime University) for providing the
341 starting material sample and Shugo Ohi (Shiga University) for help with sample preparation.
342 This work was supported by JSPS KAKENHI Grant Numbers JP16H06348 to AM.
343

References

Balzar, D., and Ledbetter, H. (1993) Crystal structure and compressibility of 3:2 mullite. American Mineralogist, 78, 1192–1196.

Bish, D.L., and Burnham, C.W. (1992) Rietveld refinement of the crystal structure of fibrolitic silliamnite using neutron powder diffraction data. American Mineralogist, 77, 374–379.

Burnham, C.W. (1963) Refinement of the crystal structure of sillimanite. Zeitschrift für Kristallographie, 118, 127–148.

Buseck, P.R., and Self, P. (1992) Electron energy-loss spectroscopy (EELS) and electron channelling (ALCHEMI). Reviews in Mineralogy and Geochemistry, 27, 141–180.

Fraser, G., McDougall, I., Ellis, D.J., and Williams, I.S. (2000) Timing and rate of isothermal decompression in Pan-African granulites from Rundvågshetta, East Antarctica. Journal of Metamorphic Geology, 18, 441-454.

Greenwood, H.J. (1972) AlIV -SiIV disorder in sillimanite and itseffect on phase relations of the aluminum silicate minerals. Geological Society of America, Memoir, 132, 553–571.

Harley, S.L. (1998) An appraisal of peak temperatures and thermal histories in ultrahigh-temperature (UHT) crustal metamorphism: the significance of aluminous orthopyroxene. Memoirs of National Institute of Polar Research Special issue, 53, 49-73.

Holdaway, M.J. (1971) Stability of andalusite and the aluminum silicate phase diagram. American Journal of Science. 271, 97–131.

366 Holland, T.J.B., and Carpenter, M.A. (1986) Aluminium/ silicon disordering and melting in
367 sillimanite at high pressures. Nature, 320, 151–153.
368 Igami, Y., Ohi, S., and Miyake, A. (2017) Sillimanite–mullite transformation observed in
369 synchrotron X-ray diffraction experiments. Journal of the American Ceramic
370 Society, 100, 4928–4937.
371 Jones, J.B. (1968) Al–O and Si–O tetrahedral distances in aluminosilicate framework
372 structures. Acta Crystallographica Section B: Structural Crystallography and Crystal
373 Chemistry, 24, 355-358.
374 Kawasaki, T., Ishikawa, M., and Motoyoshi, Y. (1993) A preliminary report on
375 cordierite-bearing assemblages from Rundvågshetta, Lützow-Holm Bay, East
376 Antarctica: Evidence for a decompressional P-T path? Proceedings of NIPR
377 Symposium of Antarctic Geosciences, 6, 47–56.
378 Kawasaki, T., Nakano, N., and Osanai, Y. (2011) Osumilite and a spinel + quartz
379 association in garnet–sillimanite gneiss from Rundvågshetta, Lützow-Holm
380 Complex, East Antarctica. Gondwana Research, 19, 430-445.
381 Matsumura, S., Soeda, T., Zaluzec, N.J., and Kinoshita, C. (2001) Electron channeling
382 X-ray microanalysis for cation configuration in irradiated magnesium alminate
383 spinel. Advances in Materials Problem Solving with the Electron Microscope,
384 129-134.
385 Muto, S., and Ohtsuka, M. (2017) High-precision quantitative atomic-site-analysis of
386 functional dopants in crystalline materials by electron-channelling-enhanced
387 microanalysis. Progress in Crystal Growth and Characterization of Materials, 63,

40–61.

Navrotsky, A., Newton, R.C., and Kleppa, O.J. (1973) Sillimanite-disordering enthalpy by calorimetry. Geochimica et Cosmochimica Acta, 37, 2497–2508.

Oxley, M.P., and Allen, L.J. (2003) ICSC: a program for calculating inelastic scattering cross sections for fast electron incident on crystals. Journal of Applied Crystallography, 36, 940–943

Peterson, R.C., and McMullan, R.K. (1986) Neutron diffraction studies of sillimanite. American Mineralogist, 71, 742–745.

Rahman, S., Feustel, U., and Freimann, S. (2001) Structure description of the thermic phase transformation sillimanite–mullite. Journal of the European Ceramic Society, 21, 2471–2478.

Raterron, P., Carpenter, M., and Doukhan, J.C. (1999) Sillimanite miullitization: ATEM investigation and point defect model. Phase Transitions, 68, 451–500.

Raterron, P., Carpenter, M., and Doukhan, J.C. (2000) ATEM investigation of experimentally annealed sillimanite: new constraints for the SiO_2 - Al_2O_3 join. Mineralogical Magazine, 64, 247-254.

Sheldrick, G.M. (1997) SHELX-97: Programs for crystal structure analysis. Göttingen, Germany.

Smith, J.V., and Bailey, S.W. (1963) Second Review of A1-O and Si-O Tetrahedral Distances. Acta Crystallographica, 16, 801–811.

Soeda, T., Matsumura, S., Kinoshita, C., and Zaluzec, N.J. (2000) Cation disordering in magnesium aluminate spinel crystals induced by electron or ion irradiation. Journal

of Neuclear Materials, 283–287, 952–956.

Spence, J.C.H., and Taftø, J. (1983) ALCHEMI: a new technique for locating atoms in small crystals. Journal of Microscopy, 130, 147–154.

Tomba, A., Camerucci, M.A., Urretavizcaya, G., Cavalieri, A.L., and Sainz, M.A. (1999) Elongated mullite crystals obtained from high temperature transformation of sillimanite. Ceramic International, 25, 245–252.

Tsuda, K., and Tanaka, M. (1999) Refinement of crystal structural parameters using two-dimensional energy-filtered CBED patterns. Acta Crystallographica Section A: Foundations of Crystallography, 55, 939–954.

Winter, J.K., and Ghose, S. (1979). Thermal expansion and high-temperature crystal chemistry of the Al_2SiO_5 polymorphs. American Mineralogist, 64, 573-586.

Yasuda, K., Yamamoto, T., Shimada, M., Matsumura, S., Chimi, Y., and Ishikawa, N. (2006) Nuclear Instruments and Methods in Physics Research B, 250, 238–244.

Yasuda, K., Yamamoto, T., and Matsumura, S. (2007) The Atomic Structure of Disordered Ion Tracks in Magnesium Aluminate Spinel. Journal of Materials, 59, 27–30.

Zen, E. (1969) The stability relations of the polymorphs of aluminum silicates: a survey and some comments. American Journal of Science. 267, 297–309.

Figure captions

Tables

Table 1. Details and results of the single X-ray diffraction measurement of the starting material

Table 2. Atomic coordinates of the starting material from the single X-ray diffraction measurement

Table 3. Average distances of the four T–O bonds in Al/SiO_4 tetrahedra

Table 4. Order parameter Q from individual measurements of the starting material

Table 5. Order parameter Q in annealed sillimanite

Figures

Figure 1. Schematic illustrations of HARECXS experiment. Electron beam is tilted to one direction (along the systematic raw reflections of 101), keeping the pivot point on the measurement region. The characteristic X-ray intensities are obtained with respect to the tilting angle.

Figure 2. Channeling plane and diffraction condition for the HARECXS experiments of this study. (a) The channeling plane (202) in crystal structure of ordered sillimanite. Only AlO_4 and SiO_4 tetrahedra are drawn in this figure. On the (202) planes, AlO_4 or SiO_4 tetrahedra are arranged separately in ordered sillimanite, but are mixed in disordered sillimanite. (b) An example of diffraction patterns at suitable diffraction conditions.

Figure 3. Average T–O distances in tetrahedra and estimated Al content in tetrahedral sites. The data of Burnham (1963) are plotted as perfectly ordered sillimanite in which Al content is zero in the Si site and 1 in the Al2 site. Solid line represents the linear relationship between Al contents and bond distances ($y = 6.4516x - 10.418$).

Figure 4. TEM image and SAED pattern of starting material. (b) is enlargement of the dashed outline in (a). Characteristic microtextures are absent in the TEM image, and the SAED pattern (inset of b) shows l = odd reflections.

Figure 5. TEM images and SAED pattern of a sample heated at 1530 °C for 5 h. Dark field TEM image taken from 111 reflection of sillimanite (a) shows dark contrast regions. Bright field image of the dashed outline (b) shows small inclusions elongated with the *c*-axis of the host sillimanite, which are similar to textures of mullite formation observed by previous studies (e.g., Raterron et al. 1999, 2000; Rahman et al. 2001). SAED pattern (inset of a) shows l = odd reflections.

Figure 6. Examples of HARECXS profiles and CBED patterns obtained from the starting material. Dotted lines show the linear combination profiles with Q = 1, 0.9, 0.8, …, 0. Solid lines show the profiles with optimized Q.

Figure 7. Histograms of the Q values determined for the starting material with (**a**) no λ_{ABS} addition, (**b**) λ_{ABS} = 3000 Å, (**c**) λ_{ABS} = 2500 Å, and (**d**) λ_{ABS} = 2000 Å.

Figure 8. HARECXS profiles and CBED patterns obtained from sillimanite annealed at 1476 °C for 90 h (left) and at 1530 °C for 5 h (right). Dotted lines show the linear combination profiles with Q = 1, 0.9, 0.8, …, 0. Solid lines show the profiles with optimized Q.

Figure 9. Values of Q determined by the HARECXS method plotted against annealing temperature (circles). The solid line shows predicted Q values determined by least-squares fitting with the Bragg-Williams model, and the region between the dotted lines is the range of Q values predicted by Greenwood (1972). The cross indicates the starting material, plotted by applying the average Q of 0.88 to the determined Bragg-Williams Q–T curve and corresponding to a temperature of ~1000 °C for the starting material.

This is a preprint, the final version is subject to change, of the American Mineralogist (MSA)
Cite as Authors (Year) Title. American Mineralogist, in press.
DOI: https://doi.org/10.2138/am-2018-6351

sample	Sillimanite
Crystal data	
Chemical formula	Al_2SiO_5
Cell weight	648.20
Crystal system, space group	Orthorhonbic, *Pbnm*
Temperature (K)	300 (Room temperature)
a, b, c (A°)	7.4867(6), 7.6750(5), 5.7720(5)
α, β, γ (°)	90, 90, 90
V (A° ^{3})	331.66
Z	4
F (000)	320.0
D_x (Mg m^{-3})	3.245
μ (mm^{-1})	1.12
Crystal shape	Block
Color	Colorless
Crystal size (μm)	80 × 80 × 60
Data collection	
Diffractometer	Rigaku, AFC-7S
Radiation source	Sealed Tube
Total reflections measured	1206
Independent reflections	527
Observed reflections	413
R_{int}	0.049
θ values (°)	θ_{max} = 60.0, θ_{min} = 3.0
$(\sin\theta/\lambda)_{max}$ (A°$^{-1}$)	0.7035
Range of *h, k, l*	h = -10→10, k = 0→10, l = 0→8
Refinement	
Refinement on	F
R 1	0.0319
R (all)	0.0429
wR 2	0.0749
GooF(obs)	1.082
GooF(all)	1.082
No. of reflections($F_o > 4\sigma(F_o)$)	413
No. of parameters	49
Weighting scheme	$w = 1/[(\sigma^2(F_o^2) + (0.0144P)^2 + 0.00\,P\,]$, where $P = [\mathrm{Max}(F_o^2, 0) + 2(F_c^2)]/3$
$(\Delta/\sigma)_{max}$	0.00
$\Delta\rho_{max}$, $\Delta\rho_{min}$ (e A°$^{-3}$)	0.41, -1.05

This is a preprint, the final version is subject to change, of the American Mineralogist (MSA)
Cite as Authors (Year) Title. American Mineralogist, in press.
DOI: https://doi.org/10.2138/am-2018-6351

Site	Occ	*x*	*y*	*z*	U_{11}	U_{22}
Al1	1	0	0	0	0.0064(3)	0.0053(3)
Al2	0.968(4)	0.14181(8)	0.34503(7)	0.25	0.0056(4)	0.0047(4)
Si	0.965(4)	0.15336(8)	0.34035(7)	0.75	0.0048(3)	0.0038(3)
O1	1	0.36044(18)	0.40921(19)	0.75	0.0069(6)	0.0099(7)
O2	1	0.35646(19)	0.43384(19)	0.25	0.0080(7)	0.0076(6)
O3	1	0.4766(2)	0.00129(16)	0.75	0.0123(8)	0.0092(7)
O4	1	0.12569(16)	0.22326(13)	0.51458(17)	0.0093(5)	0.0066(5)

This is a preprint, the final version is subject to change, of the American Mineralogist (MSA)
Cite as Authors (Year) Title. American Mineralogist, in press.
DOI: https://doi.org/10.2138/am-2018-6351

U_{33}	U_{23}	U_{13}	U_{12}
0.0064(4)	-0.0002(2)	0.0002(2)	-0.0001(2)
0.0042(4)	0	0	-0.0007(3)
0.0046(4)	0	0	-0.0002(3)
0.0045(8)	0	0	-0.0009(6)
0.0046(8)	0	0	0.0006(6)
0.0151(10)	0	0	-0.0038(6)
0.0070(5)	-0.0005(4)	-0.0003(4)	-0.0016(5)

This is a preprint, the final version is subject to change, of the American Mineralogist (MSA)
Cite as Authors (Year) Title. American Mineralogist, in press.
DOI: https://doi.org/10.2138/am-2018-6351

	Average bond distance (Å)		
	Al2 – O	**Si – O**	**Remarks**
Burnham (1963)	1.770(2)	1.615(3)	single crystal XRD
Winter & Ghose (1976)	1.764(5)	1.626(5)	single crystal XRD
Peterson & McMullan (1986)	1.759(3)	1.623(2)	single crystal ND
Bish & Burnham (1992)	1.753(4)	1.634(3)	powder ND fibrolitic sillimanite
This study	1.761(3)	1.624(3)	single crystal XRD

This is a preprint, the final version is subject to change, of the American Mineralogist (MSA)
Cite as Authors (Year) Title. American Mineralogist, in press.
DOI: https://doi.org/10.2138/am-2018-6351

Measurement No.	Thickness (nm)	Degree of order *Q*			
		No λ_{ABS} addition	λ_{ABS} = 3000 Å	λ_{ABS} = 2500 Å	λ_{ABS} = 2000 Å
1	252	0.79(3)	0.87(3)	0.88(3)	0.90(3)
2	292	0.75(2)	0.82(2)	0.84(2)	0.86(2)
3	222	0.75(2)	0.82(2)	0.84(2)	0.86(2)
4	272	0.80(3)	0.88(3)	0.89(3)	0.92(3)
5	249	0.76(2)	0.83(2)	0.85(2)	0.87(2)
6	289	0.73(2)	0.80(2)	0.82(2)	0.84(2)
7	199	0.77(2)	0.83(2)	0.85(2)	0.87(2)
8	269	0.73(2)	0.80(2)	0.82(2)	0.84(2)
9	178	0.80(2)	0.86(2)	0.88(2)	0.90(2)
10	75	0.93(4)	0.96(4)	0.96(4)	0.97(4)
11	175	0.85(2)	0.92(2)	0.93(2)	0.95(2)
12	350	0.78(2)	0.86(2)	0.88(2)	0.90(2)
13	166	0.87(2)	0.94(2)	0.95(2)	0.97(2)
14	74	0.90(3)	0.93(3)	0.94(3)	0.94(3)
15	355	0.79(2)	0.87(2)	0.89(2)	0.91(2)
16	348	0.76(2)	0.84(3)	0.85(3)	0.88(3)
17	174	0.77(2)	0.83(3)	0.85(3)	0.87(3)
18	73	0.86(4)	0.91(5)	0.92(5)	0.94(5)
Mean		0.80	0.87	0.88	0.90
Standard error		0.01	0.01	0.01	0.01

This is a preprint, the final version is subject to change, of the American Mineralogist (MSA)
Cite as Authors (Year) Title. American Mineralogist, in press.
DOI: https://doi.org/10.2138/am-2018-6351

Annealing condition		Measurement no.	Thickness (nm)	Order parameter *Q*
T (°C)	Time (h)			
1530	5	1	147	0.55(2)
		2	113	0.61(3)
1476	90	1	314	0.74(3)
		2	314	0.68(2)
		3	304	0.68(2)
1373	300	1	234	0.79(2)
1140	1512	1	261	0.79(2)
		2	261	0.82(3)
1090	1255	1	304	0.84(2)
		2	237	0.86(2)
		3	345	0.85(2)
Staring Material		1 – 18	73 – 355	0.88(1)*

* Average and standard srror of 18 measurements.

This is a preprint, the final version is subject to change, of the American Mineralogist (MSA)
Cite as Authors (Year) Title. American Mineralogist, in press.
DOI: https://doi.org/10.2138/am-2018-6351

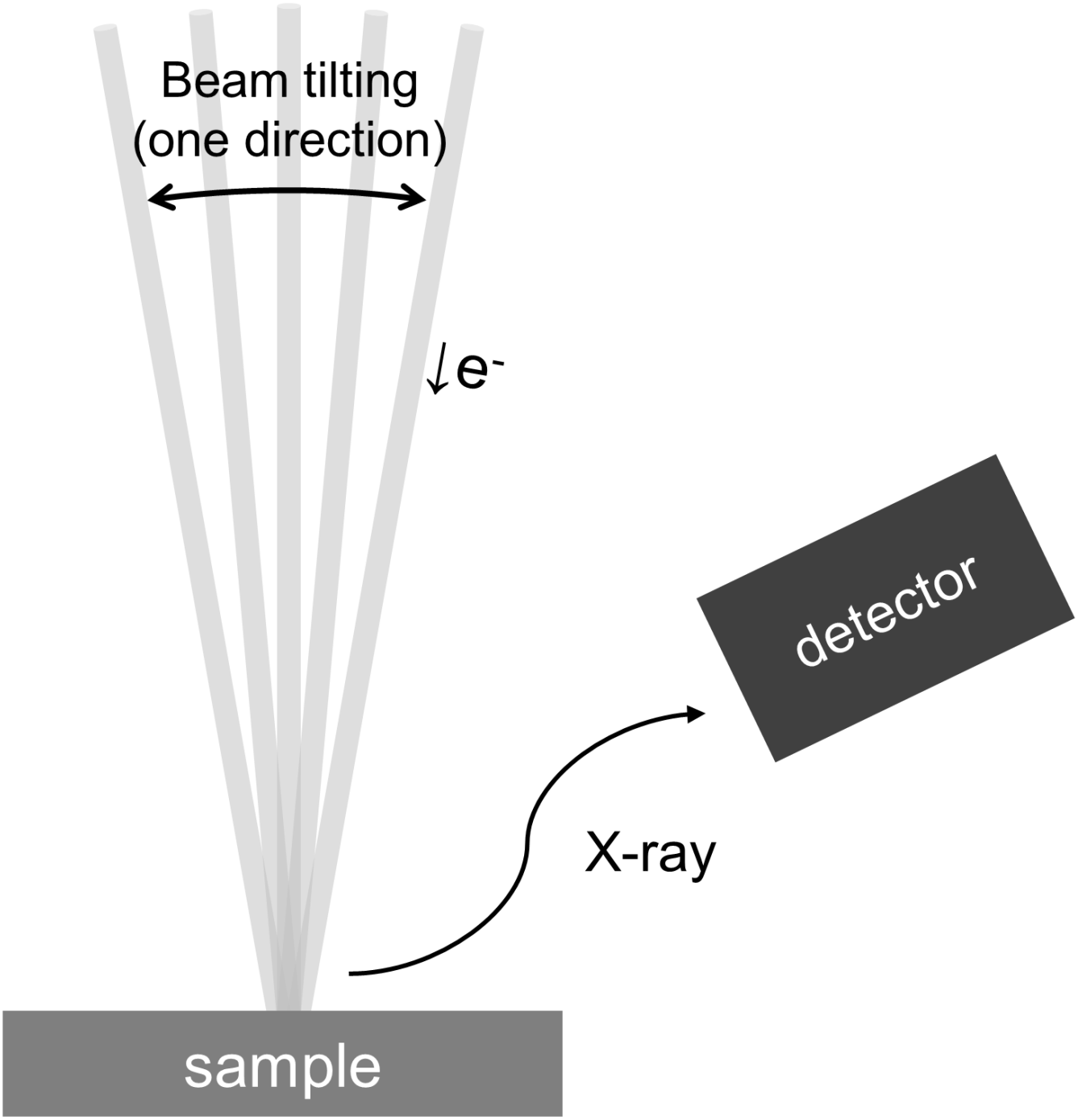

Figure 1

This is a preprint, the final version is subject to change, of the American Mineralogist (MSA)
Cite as Authors (Year) Title. American Mineralogist, in press.
DOI: https://doi.org/10.2138/am-2018-6351

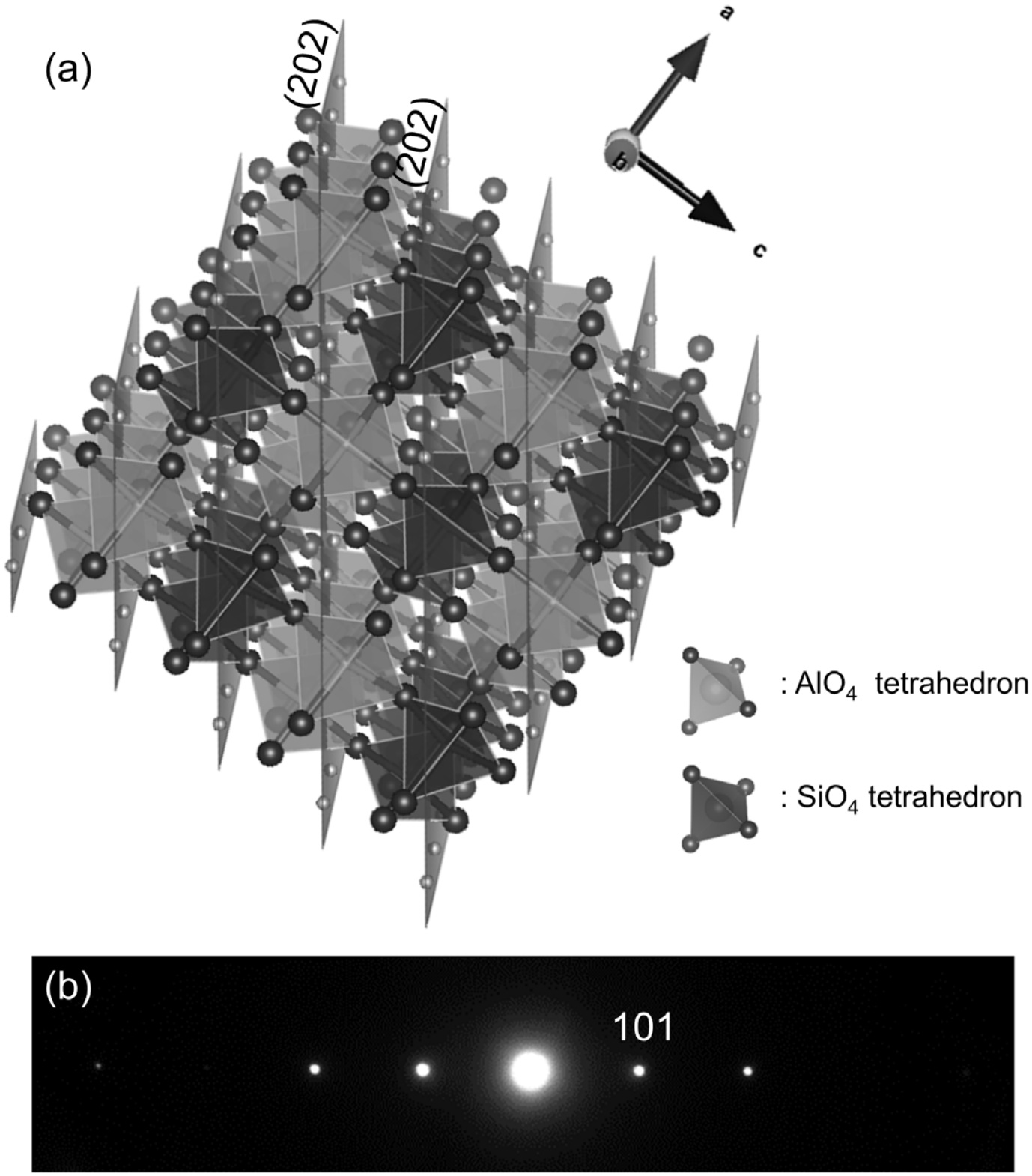

Figure 2

This is a preprint, the final version is subject to change, of the American Mineralogist (MSA)
Cite as Authors (Year) Title. American Mineralogist, in press.
DOI: https://doi.org/10.2138/am-2018-6351

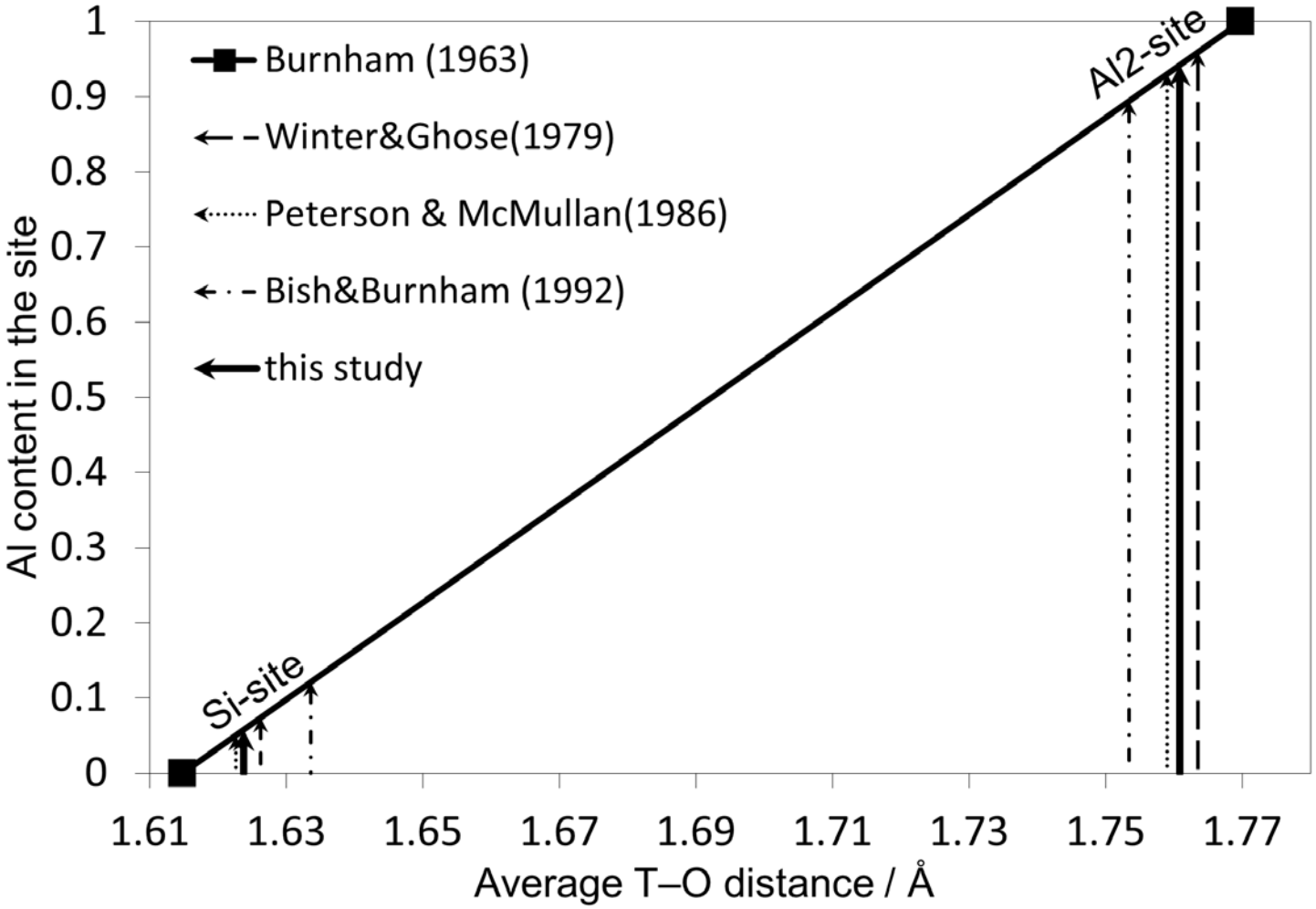

Figure 3

This is a preprint, the final version is subject to change, of the American Mineralogist (MSA)
Cite as Authors (Year) Title. American Mineralogist, in press.
DOI: https://doi.org/10.2138/am-2018-6351

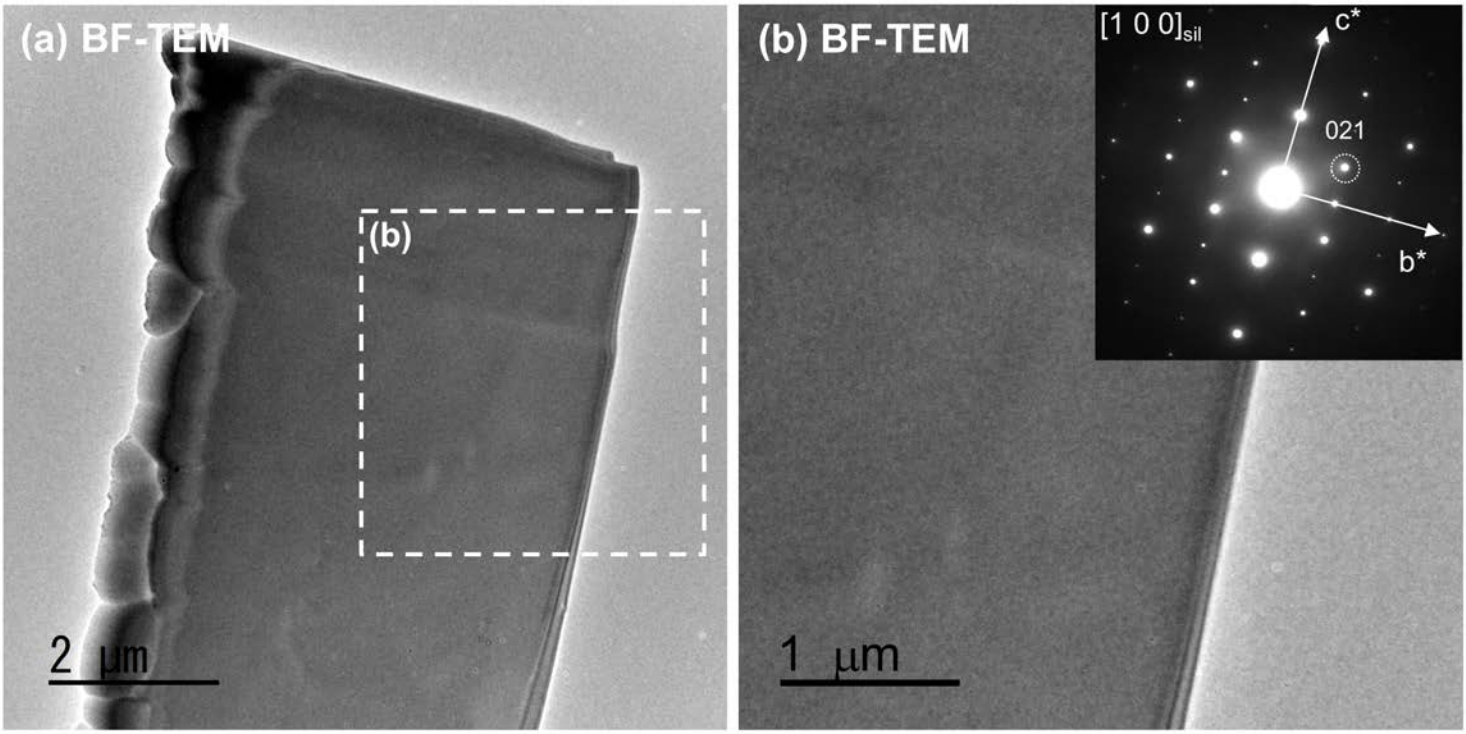

Figure 4

This is a preprint, the final version is subject to change, of the American Mineralogist (MSA)
Cite as Authors (Year) Title. American Mineralogist, in press.
DOI: https://doi.org/10.2138/am-2018-6351

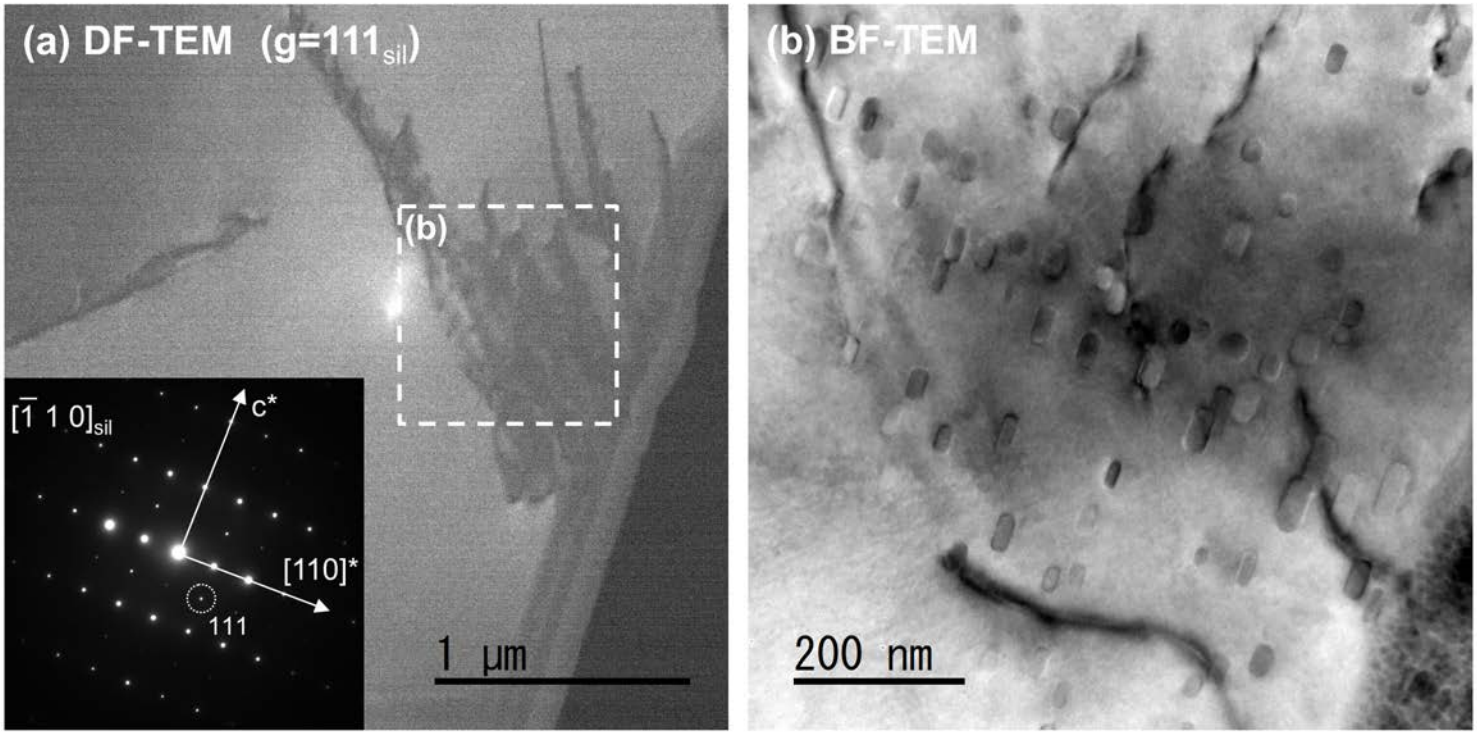

Figure 5

This is a preprint, the final version is subject to change, of the American Mineralogist (MSA)
Cite as Authors (Year) Title. American Mineralogist, in press.
DOI: https://doi.org/10.2138/am-2018-6351

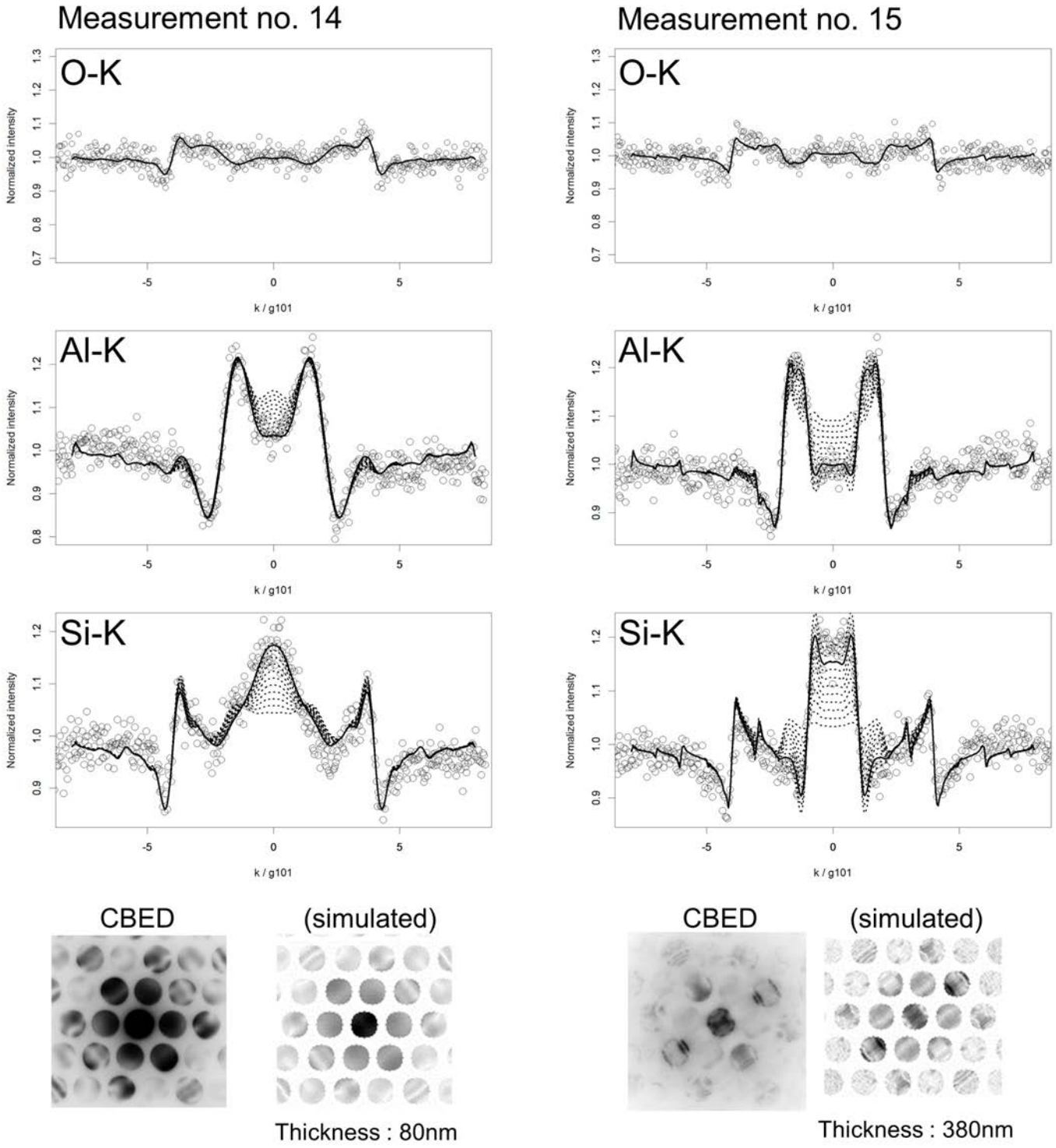

Figure 6

This is a preprint, the final version is subject to change, of the American Mineralogist (MSA)
Cite as Authors (Year) Title. American Mineralogist, in press.
DOI: https://doi.org/10.2138/am-2018-6351

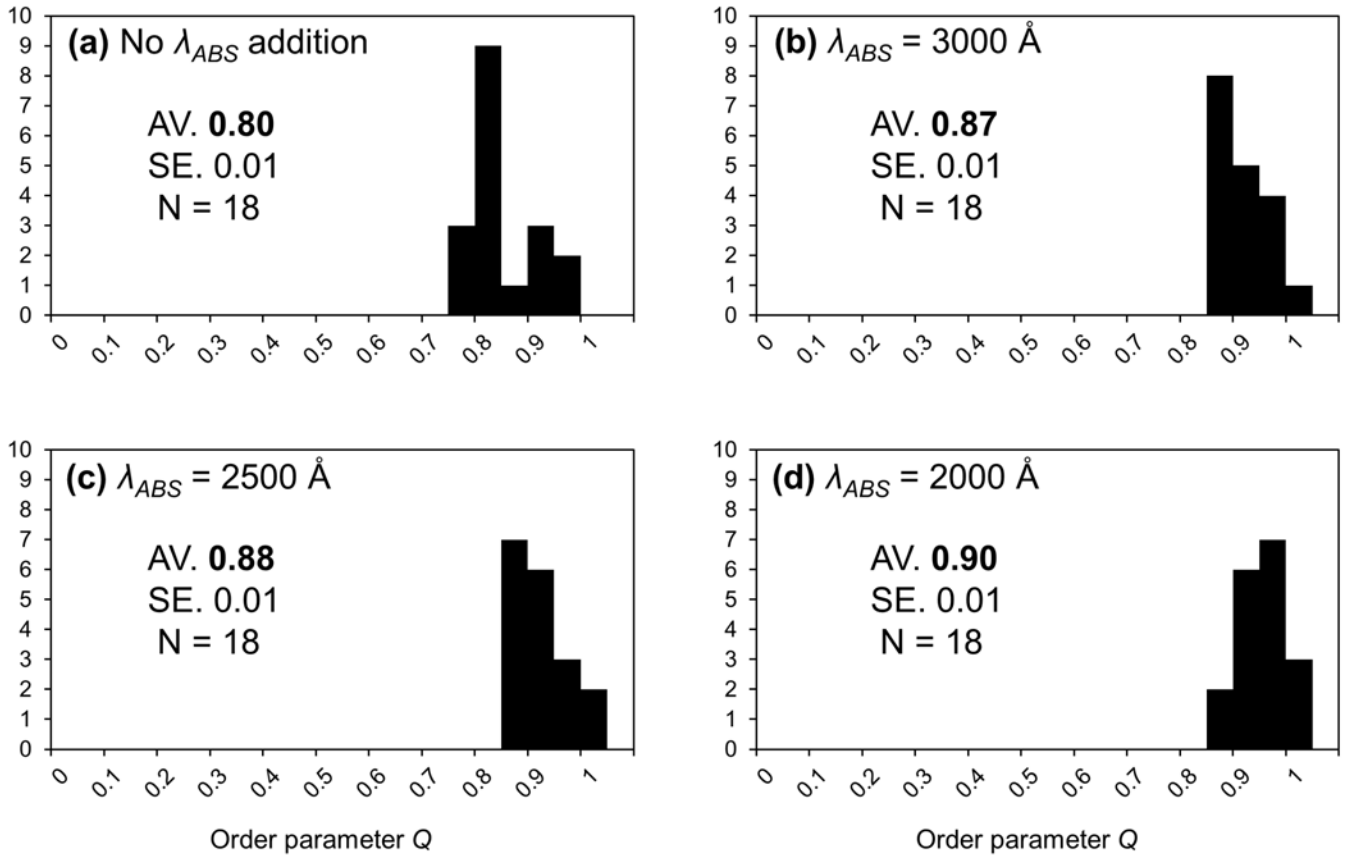

Figure 7

This is a preprint, the final version is subject to change, of the American Mineralogist (MSA)
Cite as Authors (Year) Title. American Mineralogist, in press.
DOI: https://doi.org/10.2138/am-2018-6351

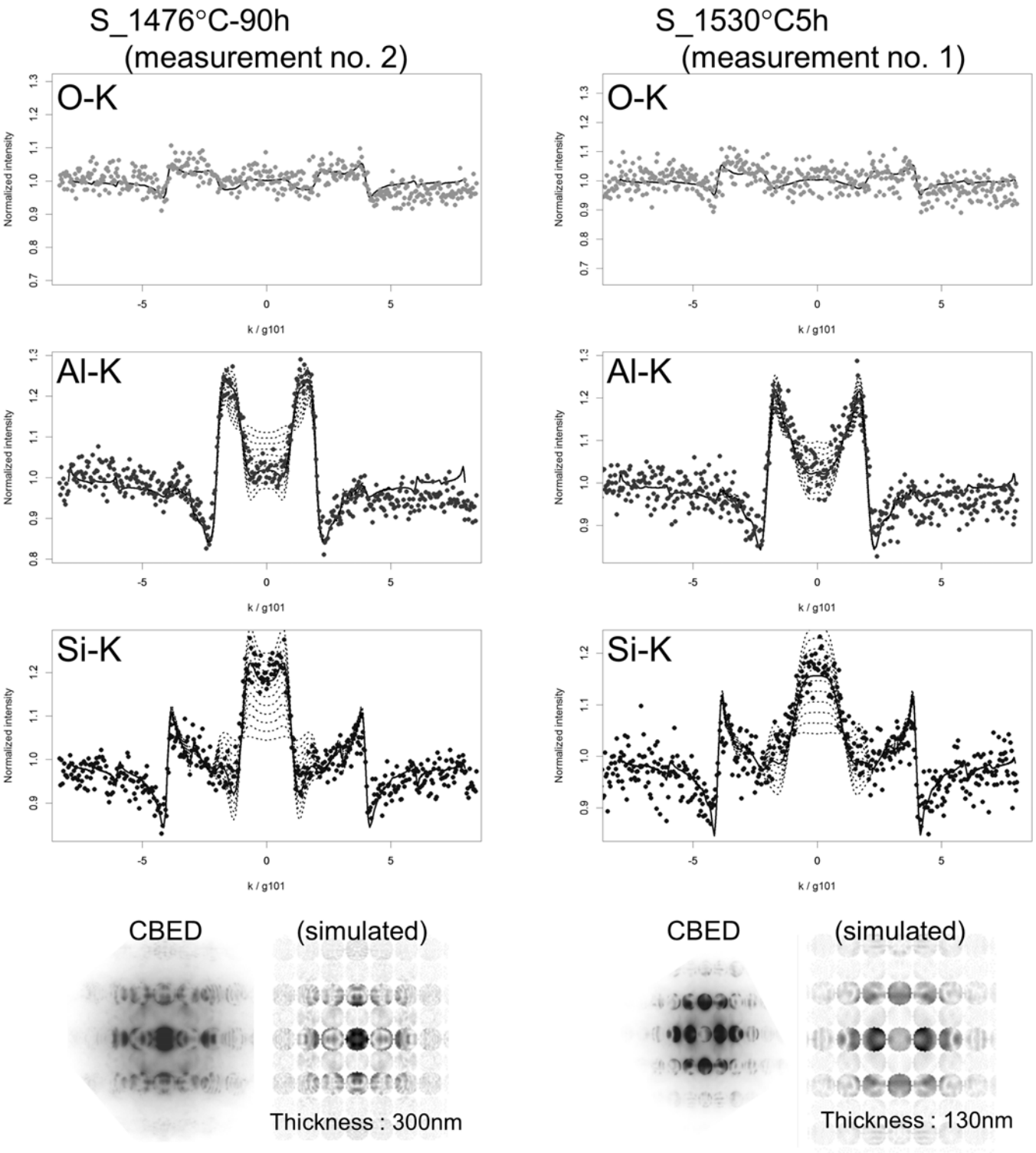

Figure 8

This is a preprint, the final version is subject to change, of the American Mineralogist (MSA)
Cite as Authors (Year) Title. American Mineralogist, in press.
DOI: https://doi.org/10.2138/am-2018-6351

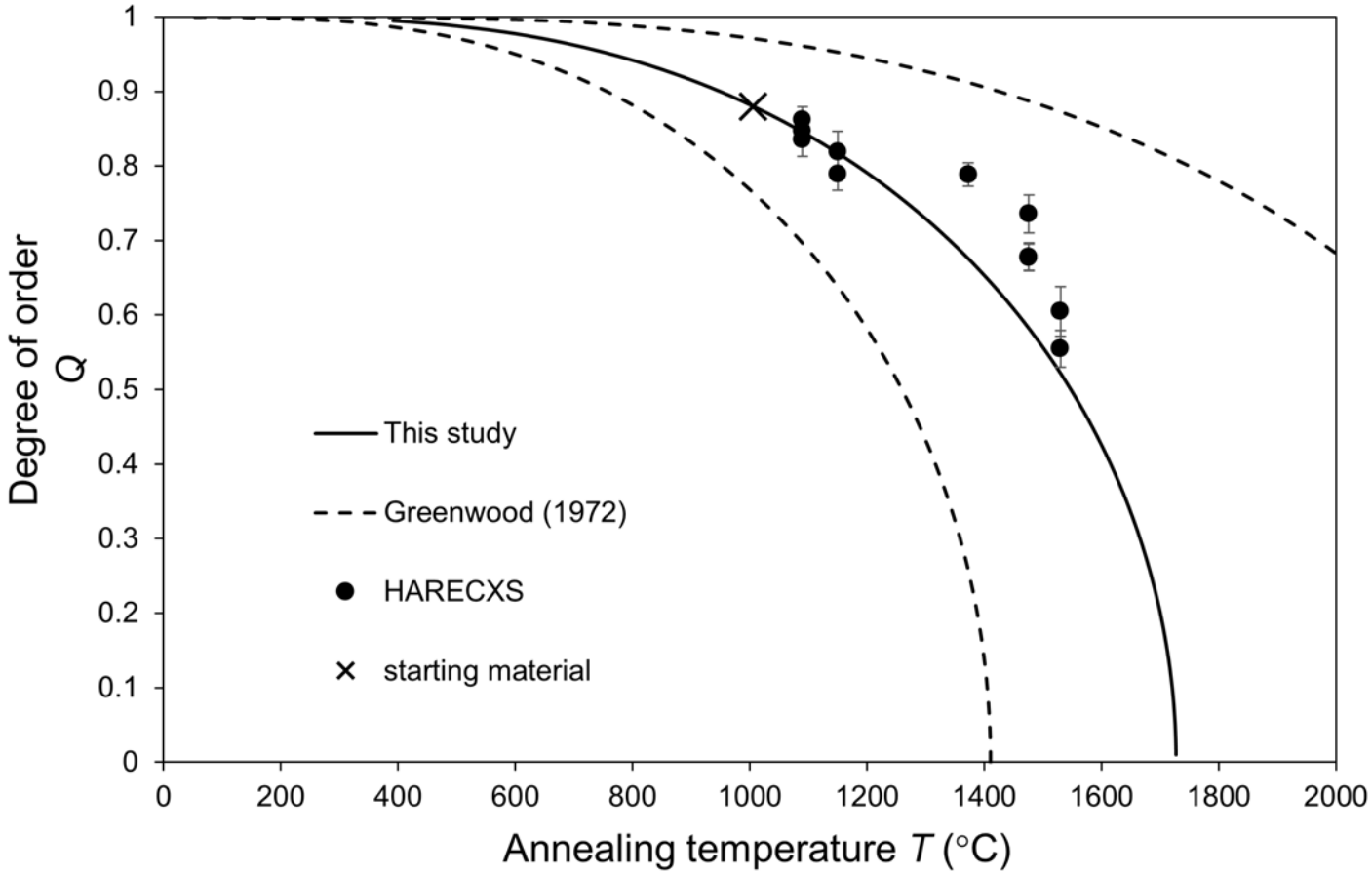

Figure 9